Photoabsorption spectrum of helium trimer cation-Theoretical modeling

René Kalus, Frantisek Karlický, Bruno Lepetit, Ivana Paidarová, Florent X. Gadéa

Photoabsorption spectrum of helium trimer cation—Theoretical modeling

René Kalus' , František Karlický, Bruno Lepetit, Ivana Paidarová, and Florent Xavier Gadea

Citation: J. Chem. Phys. **139**, 204310 (2013); doi: 10.1063/1.4832736
View online: http://dx.doi.org/10.1063/1.4832736
View Table of Contents: http://aip.scitation.org/toc/jcp/139/20
Published by the American Institute of Physics

Photoabsorption spectrum of helium trimer cation—Theoretical modeling

René Kalus,[1,a)] František Karlický,[2] Bruno Lepetit,[3] Ivana Paidarová,[4] and Florent Xavier Gadea[5]

[1]*Centre of Excellence IT4Innovations and Department of Applied Mathematics, VSB-Technical University of Ostrava, 17. listopadu 15, 708 33 Ostrava, Czech Republic*
[2]*Regional Centre of Advanced Technologies and Materials and Department of Physical Chemistry, Faculty of Science, Palacký University, Tř. 17. listopadu 12, 771 46 Olomouc, Czech Republic*
[3]*Laboratoire Collisions Agrégats Réactivité, IRSAMC & UMR5589 du CNRS, Université de Toulouse, UPS, 118 route de Narbonne, 31062 Toulouse Cedex, France*
[4]*J. Heyrovský Institute of Physical Chemistry, ASCR, v.v.i., Dolejškova 3, 182 23 Praha, Czech Republic*
[5]*Laboratoire de Chimie et de Physique Quantiques, IRSAMC & UMR5626 du CNRS, Université de Toulouse, UPS, 118 route de Narbonne, 31062 Toulouse Cedex, France*

(Received 29 July 2013; accepted 8 November 2013; published online 27 November 2013)

The photoabsorption spectrum of He_3^+ is calculated for two semiempirical models of intracluster interactions and compared with available experimental data reported in the middle UV range [H. Haberland and B. von Issendorff, J. Chem. Phys. **102**, 8773 (1995)]. Nuclear delocalization effects are investigated via several approaches comprising quantum samplings using either exact or approximate (harmonic) nuclear wavefunctions, as well as classical samplings based on the Monte Carlo methodology. Good agreement with the experiment is achieved for the model by Knowles *et al.*, [Mol. Phys. **85**, 243 (1995); Mol. Phys. **87**, 827 (1996)] whereas the model by Calvo *et al.*, [J. Chem. Phys. **135**, 124308 (2011)] exhibits non-negligible deviations from the experiment. Predictions of far UV absorption spectrum of He_3^+, for which no experimental data are presently available, are reported for both models and compared to each other as well as to the photoabsorption spectrum of He_2^+. A simple semiempirical point-charge approximation for calculating transition probabilities is shown to perform well for He_3^+. © *2013 AIP Publishing LLC*. [http://dx.doi.org/10.1063/1.4832736]

I. INTRODUCTION

Photoabsorption and subsequent photofragmentation represent well established experimental tools for studying the electronic structure of atomic and molecular complexes. They primarily provide information on electronic states of the system under study and its non-adiabatic dynamics following initial excitation. Unfortunately, the information provided by photofragmentation experiments is usually indirect and a proper theoretical interpretation is needed to get a clear picture. Numerical simulations play a very important role in the interpretation of photoabsorption and photofragmentation data and have become a common tool during last two decades, in particular as a consequence of the exponentially growing power of available computers.

The photoabsorption and photofragmentation based methods have been successfully applied, among others, to rare-gas cluster cations, Rg_N^+, and a lot of experimental papers investigating their photoabsorption and photodissociation[1] have been published, mostly in the 1990s (see, e.g., Refs. 2–6). The rare-gas cluster cations have also received a considerable attention from the theory.[7–16] The following reasons may justify their attractiveness for theoreticians. First of all, the electronic structure of Rg_N^+ can be realistically modeled via computationally cheap semiempirical methods based on the *diatomics-in-molecule* (DIM) approach[17] which have been recently shown to be highly accurate and comparable to high-level quantum chemistry approaches[18] like, e.g., the coupled clusters or multireference configuration interaction methods. Noteworthy, not only the electronic ground state, but also plethora of excited states covering a broad range of electronic excitations from infrared to ultraviolet are provided by these models. In addition, the most important relativistic effects, the spin-orbit coupling, can be included in the DIM approach[19] via a simple and still highly accurate *atoms-in-molecules* approximation.[20] Despite all these facts, many problems that emerged from the experiments performed on Rg_N^+ have still not been solved and the understanding of many features of the complex post-excitation dynamics of Rg_N^+, including their photodynamics, is still far from perfection. This holds, in particular, for helium cluster cations for which, for example, detailed photoabsorption and photofragmentation experiments were performed almost 20 years ago[6] and still have not received any theoretical response.

The helium cluster cations, He_N^+, represent an exception among the rare-gas cluster cations since it has been known for long that the original DIM approach does not work for them as it usually does for the other Rg_N^+. A well known failure of the DIM model for helium is that it is not even able to reproduce the equilibrium geometry of He_3^+ in its electronic ground state.[21,22] While a linear symmetric structure is predicted by highly correlated *ab initio* methods, a linear asymmetric structure is favored by all the pure DIM

a)Electronic mail: Rene.Kalus@vsb.cz

models, regardless of their level and accuracy. This defect was attributed to the lack of three-body interactions in the pure DIM approach[21] and a couple of modifications were proposed for He_N^+ to improve the performance of the DIM model for them. The modifications can be divided in two major groups: (a) approaches which modify the diatomic curves (which are independent inputs to the DIM models), in particular the diatomic potential for neutral He_2, so that the correct equilibrium structure of He_3^+ is reproduced[23] and (b) approaches which add explicit three-body corrections derived from accurate *ab initio* calculations on He_3^+ into the DIM Hamiltonian for He_N^+ .[21] Both approaches have been used in the past in developing extended DIM models for He_N^+ and state-of-the-art representatives of these modified DIM approaches are, respectively, (a) the model developed recently by Calvo *et al.*[24] and (b) the model proposed in 1990s by Knowles *et al.*[21,25] A primary aim of the present work is to test the reliability of the two semiempirical models by calculating the photoabsorption spectrum of He_3^+ and by comparing the theoretical predictions with available experimental data.[6] These tests should serve as a first step towards a reliable modeling of the photoabsorption spectra of larger He_N^+ and their photodynamics, which is intended for future studies.

The present paper is organized as follows. First, the methods employed and computational details are briefly summarized in Sec. II with a special focus on three basic ingredients of the photoabsorption modeling: interaction models (Subsection II A), electronic transition probabilities (Subsection II B), and nuclear delocalization effects modeling (Subsection II C). Then, the main computational results are given for the two interaction models considered in this work in Sec. III. First, a detailed analysis is performed for the middle ultraviolet (mid-UV) range where experimental data are available in Subsection III A, and then photoabsorption profiles of He_3^+ are presented in the far-UV range in Subsection III B. The effect of vibrational and rotational excitations on the photoabsorption of He_3^+ is further briefly discussed in Subsection III C. Finally, conclusive remarks and prospects are given in Sec. IV.

II. METHODS AND COMPUTATIONS

The photoabsorption cross-section can be calculated for photons of energy E exciting a system from its electronic ground state to one of the excited states via Refs. 12 and 26 (see also pioneering Refs. 27 and 28, or Ref. 29 for a more comprehensive survey)

$$\sigma(E) = \lim_{\Delta E \to 0} \frac{1}{\Delta E} \frac{\pi}{3\varepsilon_0 c\hbar} \frac{\sum_{\mathcal{K}=1}^{\mathcal{N}} \sum_a w_{\mathcal{K}} (E_a(\mathbf{R}^{(\mathcal{K})}) - E_0(\mathbf{R}^{(\mathcal{K})})) |\mu_{0a}(\mathbf{R}^{(\mathcal{K})})|^2}{\sum_{\mathcal{K}=1}^{\mathcal{N}} w_{\mathcal{K}}}, \quad (1)$$

where ε_0, c, and $\hbar$ are the vacuum permittivity, vacuum light velocity, and the Planck constant, respectively, E_a denotes the energy of electronic state a (E_0 corresponds to the electronic ground state), μ_{0a} is the transition dipole moment for the $0 \rightarrow a$ transition, all the three quantities being calculated over a set of $\mathcal{N}$ nuclear configurations, $\mathbf{R}^{(\mathcal{K})}$, used to model nuclear delocalization, and $w_{\mathcal{K}}$ are non-normalized weights of the nuclear configurations corresponding to a particular sampling of the ground-state potential energy surface (PES). The first summation in the numerator of the r.h.s. of Eq. (1) and the sum in the denominator run over a representative set of nuclear configurations, and only excited states obeying $(E_a - E_0) \in [E, E + \Delta E]$ are included in the second summation in the numerator.

As a consequence, three basic ingredients are needed for calculating $\sigma(E)$ via Eq. (1): (a) an interaction model providing all relevant electronic states of the studied system, (b) a model for evaluating the transition dipole moments, and (c) a methodology for generating representative sets of nuclear configurations needed for properly averaging the semiclassical transition probabilities. In Subsections II A–II C, we briefly discuss how these ingredients are obtained in the present study on He_3^+.

A. Intracluster interactions

As already mentioned in the Introduction, the DIM model[17] has successfully been employed in various modelings of heavier rare gases (Ne–Xe), including the modeling of their photoabsorption and photodissociation. The DIM methodology consists in expanding the electronic Hamiltonian of a system containing N atoms into diatomic and atomic terms,

$$\hat{\mathrm{H}} = \sum_{J=1}^{N-1} \sum_{K=J+1}^{N} \hat{\mathrm{H}}_{JK} - (N-2) \sum_{K=1}^{N} \hat{\mathrm{H}}_K, \quad (2)$$

and in proposing a proper basis set of electronic wavefunctions for which the corresponding Hamiltonian matrix can be written in terms of diatomic and atomic energies (independent inputs to the DIM models usually taken from *ab initio* calculations or semiempirical modelings). How all this can be done for cationic clusters of heavier rare gases with *sp* valence orbitals was described in Refs. 19 and 30, the application of the DIM approach to helium cluster cations was outlined, e.g., in Refs. 21 and 23. The basis set proposed to be used together with the DIM models for the rare gases is a minimum basis set of approximately diabatic wavefunctions representing states with the positive charge localized on a particular atom. For an N-atomic helium cluster cation, totally N such wavefunctions are needed,

$$\Phi_K = |\varphi_1 \bar{\varphi}_1 \ldots \varphi_{K-1} \bar{\varphi}_{K-1} \varphi_K \varphi_{K+1} \bar{\varphi}_{K+1} \ldots \varphi_N \bar{\varphi}_N|, \quad (3)$$

where vertical bars, $|\,|$, denote a normalized Slater determinant, φ_I is a $1s$ orbital centered on atom I, and bars above φ distinguish between two spin orientations, without bar for

the "up" orientation and with bar for the "down" orientation. Noteworthy, only one spin orientation can be considered for the ionized atom since the spin-orbit coupling need not be taken into account in He_N^+. In addition, Φ_K can be considered real-valued.

This purely pair-wise additive approach to the modeling of intra-system interactions can be further improved by including polarization and dispersion three-body forces as detailed in Refs. 19 and 31, respectively.

The pure DIM methodology fails for He_N^+[21,22] even if polarization three-body forces are considered. As discussed in some detail in Sec. I, two methods were proposed to remove this defect and, presently, two state-of-the-art semiempirical interaction models, free of this defect, are reported for He_N^+ in the literature: a model developed by Knowles *et al.* in Ref. 21 and slightly corrected in Ref. 25, which is based on including three-body correction terms obtained from high-level calculations on He_3^+ in the DIM Hamiltonian, and another model developed later on by Calvo *et al.*,[24] which employs empirical modifications of the diatomic curves used in the DIM model so that they effectively include the three-body interactions. For a detailed description of the two models see cited literature. Mostly, these two models are used throughout this work and, below, they are denoted as the Knowles *et al.* model and the Calvo *et al.* model. For comparison, a pure DIM model is also considered. It is based on state-of-the-art *ab initio* diatomic curves for the electronic ground state and the first excited state of He_2^+[32] and the highly accurate curve for the electronic ground state of He_2 as proposed in Ref. 33. We denote this model simply as DIM (or pure DIM) in this work.

B. Transition dipole moment

A most important contribution to the photoabsorption cross-section (Eq. (1)) is the transition probability for the underlying electronic transition ($0 \rightarrow a$) which is proportional, within the first-order non-stationary perturbation theory, to the energy difference of the two states involved, $E_a - E_0$, and the square of the transition dipole moment between the two states,[11] $|\mu_{0a}|^2$,

$$P_{0\rightarrow a} \sim (E_a - E_0)|\mu_{0a}|^2. \tag{4}$$

The energy difference is obtained by diagonalizing the electronic Hamiltonian matrix provided by the interaction models introduced in Subsection II A, the calculation of the transition dipole moment is briefly described here.

For charged clusters of heavier rare gases (Ar–Xe), *point-charge approximation* (PCA)[10] has been successfully used in transition dipole moment calculations. For He_N^+, the transition dipole moment is obtained within the PCA as

$$\vec{\mu}_{0a}(\mathbf{R}) \approx e \sum_K C_K^{(0)*} C_K^{(a)} \vec{R}_K, \tag{5}$$

where $\vec{R}_K$ denotes the position of the atom K in the current cluster configuration $\mathbf{R}$, and $C_K^{(0)}$ and $C_K^{(a)}$ are the expansion coefficients of, respectively, the electronic ground-state wavefunction and the wavefunction of the excited state a expressed in the diabatic basis set given by Eq. (3). In a general case, asterisk denotes the complex conjugation, but need not be considered here since, as discussed in Subsection II A, the electronic Hamiltonian matrix can be assumed real-valued for He_N^+ and the expansion coefficients are thus real-valued as well.

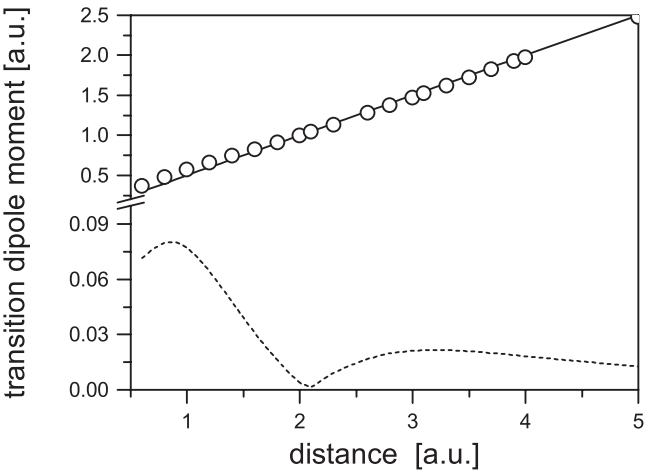

FIG. 1. Parallel transition dipole moment for He_2^+ calculated *ab initio* (circles) and approximated by the *point-charge approximation* ($R/2$) dependence (solid line). Magnitudes of differences between the *ab initio* data and the $R/2$ line are depicted in the lower part of the figure. Note the break and different scales on the vertical axis.

Despite the fact that the PCA performs rather well for rare-gas cluster cations, Naumkin pointed out in Ref. 34 that polarization of electronic clouds may play a role for these systems and developed a DIM-based methodology for including the polarization effects in PCA calculations. Later on, it was shown that this correction is particularly important for heavy rare gases (krypton and xenon) and that the extension developed by Naumkin is capable to accurately reproduce the photoabsorption spectrum of rare-gas dimers (e.g., Kr_2^+[16]) calculated at full *ab initio* level. Nevertheless, the inclusion of polarization effects does not seem to be necessary for He_N^+, mainly because light helium atoms are only weakly polarizable. To justify this conclusion, we compare in Fig. 1 the transition dipole moment, $\mu_{0\rightarrow 1}$, calculated for the dominating parallel transition in He_2^+ either *ab initio* or using PCA (which degenerates, in this case, to a simple $R/2$ dependence of $\mu_{0\rightarrow 1}$ on the interatomic distance, solid line in Fig. 1). Clearly, accurate *ab initio* calculations performed at icMRCI/aug-cc-pVQZ level using the MOLPRO package[35] (circles in Fig. 1) follow closely the $R/2$ line down to very short interatomic distances. Noteworthy, the difference is less or equal 1% even for distances around the equilibrium separation in He_2^+ ($r_{eq} \approx 2.1$ a.u.) and grows up to about 7% only for $r \approx 1.4$ a.u. However, such a short distance can be reached in electronically ground-state He_2^+ only if the dimer is vibrationally excited close to its dissociation limit. As a consequence, the simple PCA can be safely used in transition dipole moment calculations, as done throughout this work.

C. Nuclear configurations

Since nuclear delocalization plays an important role in light helium clusters, even at close-to-zero temperatures, the

transition probabilities have to be properly averaged over a representative set of nuclear configurations. There are, in principle, three ways how to model the nuclear delocalization in He_3^+, provided the cluster can be considered cold with internal temperature $T \approx 0$ K.[36] First, the most realistic way is that the configurations used in Eq. (1) are sampled from *the square of accurate vibrational ground-state wavefunction* which can be obtained for He_3^+ by numerically solving nuclear stationary Schrödinger equation on the electronic ground-state PES. Second, sampling from *the ground-state vibrational wavefunction calculated at the harmonic approximation level* represents a bit more approximate way. This approach retains the quantum treatment of the light helium nuclei, but disregards anharmonicities in the He_3^+ PES in the vicinity of the classical minimum. Third, the quantum delocalization can be, at least by part, modeled by *classical samplings* of hot (vibrationally excited) clusters instead of cold ones. In this case, the classical vibrational excitation of the cluster (classical non-zero temperature) will approximately mimic the zero-temperature quantum delocalization. All the three approaches are used in this work and compared to each other. The inclusion of the two latter, approximative approaches is motivated by the fact that the state-of-the-art calculations employing accurate vibrational wavefunctions cannot be simply extended to larger cluster sizes while the latter two can.

1. Sampling from accurate wavefunction for He_3^+ vibrational ground state

The hyperspherical method,[37,38] employed recently in calculations of He_3^+ and Ar_3^+ vibrational spectrum and Ar_3 and H_3^+ rotational-vibrational spectrum,[39–42] is used in this work to obtain the accurate wavefunction corresponding to the He_3^+ rotational-vibrational ground state. Up to numerical uncertainties, this approach is essentially free of systematic errors and we consider it as a benchmark for the other sampling methods. The photoabsorption cross-sections calculated using coordinates sampled via the hyperspherical approach are denoted below by acronym HYP.

A detailed description of the current implementation of the hyperspherical method for He_3^+ has been given in Refs. 39–42 and, thus, only brief remarks directly related to the subject of the present study are included here. In general, our implementation of the hyperspherical method consists in transforming the nuclear Schrödinger equation for a three-body system into row-orthonormal hyperspherical coordinates:[37] hyperradius (ρ) and two hyperangles (θ and δ) representing vibrational degrees of freedom, and three Euler angles (a, b, and c) describing the system rotations in the center-of-mass frame. In the discrete variable representation, values of the ground-state vibrational wavefunction, Ψ_0^{vib}, can be obtained for a non-rotating system over in principle arbitrarily large grids of ρ_{i_ρ} ($i_\rho = 1, \ldots, N_\rho$), θ_{i_θ} ($i_\theta = 1, \ldots, N_\theta$), and δ_{i_δ} ($i_\delta = 1, \ldots, N_\delta$):[43]

$$\Psi_0^{\text{vib}}(\rho_{i_\rho}, \theta_{i_\theta}, \delta_{i_\delta}) = \sum_{j=1}^{N_s} a^0_{ji_\rho} \sum_{k=1}^{N_h} c_{jk}(\rho_{i_\rho}) F_k(\theta_{i_\theta}, \delta_{i_\delta}). \quad (6)$$

A basis set of N_h principal-axes-of-inertia hyperspherical harmonics, F_k, together with ρ-dependent expansion coefficients, c_{jk}, form N_s surface functions $\Phi_j = \sum_{k=1}^{N_h} c_{jk} F_k$, which are eigenfunctions of the ρ-fixed Hamiltonian. The coefficients $a^0_{ji_\rho}$ of the expansion (Eq. (6)) are obtained by diagonalizing the matrix representation of the nuclear Hamiltonian in the product basis, the size of which is $N_\rho N_s$. Here, we choose $N_s = 45$ surface functions and $N_h = 1365$ hyperspherical harmonics following Ref. 39. $N_\rho = 272$ equispaced points have been used for $\rho \in [3 \text{ bohrs}, 15 \text{ bohrs}]$ and $N_\theta = N_\delta = 250$ points for $\theta \in [0, \pi/4]$ and $\delta \in [0, \pi]$ have been generated, respectively. In this way, totally $\mathcal{N} = 17 \times 10^6$ grid points have been considered in Eq. (1) which effectively cover all relevant parts of the He_3^+ configuration space where the ground-state vibrational wavefunction is non-negligible. Configurations of He_3^+ corresponding to the generated values of the three hyperspherical coordinates have been used in Eq. (1) with weights proportional to the product of the square of the vibrational wavefunction and the magnitude of the Jacobian for the hyperspherical to the Cartesian coordinates transition,[44]

$$w_{\mathcal{K}} \sim \left|\Psi_0^{\text{vib}}(\rho_{\mathcal{K}}, \theta_{\mathcal{K}}, \delta_{\mathcal{K}})\right|^2 \times \rho_{\mathcal{K}}^5 \sin(4\theta_{\mathcal{K}}). \quad (7)$$

2. Sampling from wavefunction calculated at the harmonic approximation level

For small vibrations around an equilibrium configuration of an N-atomic system, the harmonic approximation can be used within which the PES is approximated, in a close vicinity of the equilibrium configuration, by a simple quadratic function. In this case, the stationary Schrödinger equation can be solved analytically and the vibrational ground-state wavefunction can be expressed in normal-mode coordinates as a product of independent Gaussian functions. If equal masses are considered for all the atoms involved, the wavefunction reads as follows (see, e.g., Refs. 45 and 13):

$$\Psi_0^{\text{vib}} \sim \prod_{k=1}^{f} e^{-\frac{m\omega_k q_k^2}{2\hbar}}, \quad (8)$$

where q_k, ω_k, m, and $\hbar$ are, respectively, the normal-mode coordinates, angular frequencies, atomic mass, and Planck constant, and f is the number of vibrational modes ($f = 4$ for the equilibrium, linear symmetric structure of He_3^+[46]).

In this work, the approximate wavefunction of Eq. (8) is used to assess, by comparing with the HYP approach, the influence of anharmonic corrections to the He_3^+ PES around its linear symmetric equilibrium configuration. Below, we denote the photoabsorption data obtained for configurations sampled from the square of the harmonic vibration wavefunction by acronym HA (Harmonic Approximation). Since the normal mode coordinates can directly be sampled from Gaussian distributions corresponding to the square of the wavefunction given by Eq. (8), the sampled configurations are included in the photoabsorption cross-section calculations (Eq. (1)) with equal weights, $w_{\mathcal{K}} = 1$.

3. Classical samplings

Even though helium atoms are too light for the classical approach to be valid for them, particularly at low temperatures, classical sampling methods may still be of some use for two reasons. First of all, it is well known that increased temperature or internal energy of the system at the classical level may, at least partly, mimic quantum nuclear delocalization. Second, it can be easily shown that, for a linear harmonic oscillator, classical constant-temperature simulations should lead to a distribution of geometries corresponding exactly to the square of the ground-state vibration wavefunction if the classical temperature is chosen properly ($T_{\text{eff}} = \hbar\omega/2k_{\text{B}}$).[47] As a consequence, a classical constant-temperature simulation with properly chosen temperature may approximately reproduce the zero-temperature quantum distribution and take partly anharmonic effects into account at the same time since it is not constrained to the harmonic PES. We have included classical sampling methods in the present work as a straightforward and cheap alternative to quantum samplings for larger He_N^+ for which (a) the full quantum approach is not possible or extremely time consuming and (b) the harmonic approximation approach may fail due to anharmonicities or due to the existence of many structural isomers.

Two classical sampling methods are used in this work, the constant-temperature (canonical) Monte Carlo and the constant-energy (microcanonical) Monte Carlo method.[48] Non-rotating clusters (with zero angular momentum) are considered in the classical samplings so that the corresponding data are compatible with the data obtained from quantum calculations, which are, as well, performed for non-rotating clusters. Photoabsorption data obtained for the two classical approaches are, respectively, denoted in this work as cMCJ0 and μcMCJ0. Standard Metropolis sampling algorithm[49] is used with equilibrium distributions given by[50,51]

$$\rho(\mathbf{R})_{\text{c,J=0}} \sim \frac{1}{\sqrt{\det[\mathbf{I}(\mathbf{R})]}} \exp\left[-\frac{E_0(\mathbf{R})}{k_{\text{B}}T}\right] \tag{9}$$

for cMCJ0 and

$$\rho(\mathbf{R})_{\mu\text{c,J=0}} \sim \frac{1}{\sqrt{\det[\mathbf{I}(\mathbf{R})]}} [E_{\text{int}} - E_0(\mathbf{R})]^{\frac{f}{2}-1} \Theta[E_{\text{int}} - E_0(\mathbf{R})], \tag{10}$$

where f is the number of vibrational degrees of freedom ($f = 4$ for He_3^+), for μcMCJ0. In Eqs. (9) and (10), $E_0(\mathbf{R})$ denotes the energy of the electronic ground state of He_3^+ calculated at the configuration $\mathbf{R}$ (and normalized to zero at the classical equilibrium structure), $\det[\mathbf{I}(\mathbf{R})]$ is the determinant of the cluster inertia momentum at the configuration $\mathbf{R}$, T, and E_{int} are the cluster temperature and internal energy, respectively, and Θ denotes the Heaviside function.

Since the He_3^+ configurations are directly sampled from the distributions given in Eqs. (9) and (10) by the Metropolis algorithm, their weights are set to one in Eq. (1), $w_{\mathcal{K}} = 1$.

III. RESULTS AND DISCUSSIONS

Before presenting the calculated photoabsorption cross-sections, let us summarize the structural properties, binding energies, vertical excitation energies, and vertical transition dipole moments for equilibrium He_3^+. Such a summary will be useful for the interpretation of ensuing photoabsorption data and is done in Tables I–III where results obtained from semiempirical models are compared with recent *ab initio* data.[52]

TABLE I. Equilibrium distances and binding energies of He_3^+ calculated for semiempirical models and compared with *ab initio* values taken from Refs. 52 and 39. Energies are given in eV, distances in Å, and r_{12} and r_{23} refer to the distances between the central atom (2) and one of the two wing atoms (1 or 3) in the linear equilibrium configuration.

Model	Geometry	r_{12}–r_{23}	D_{e}	D_0
Knowles *et al.*	$D_{\infty h}$	1.241–1.241	2.659	2.546
Calvo *et al.*	$D_{\infty h}$	1.240–1.240	2.626	2.513
DIM	$C_{\infty v}$	1.084–1.996	2.512	2.395
Ab initio	$D_{\infty h}$	1.238–1.238	2.638	2.517

First, equilibrium geometries and dissociation energies are summarized for equilibrium He_3^+ in Table I. As expected, the models by Knowles *et al.* and Calvo *et al.* reproduce well the equilibrium geometry as well as the binding energy of He_3^+ while the DIM model fails. The good performance of the two former models is not surprising since the model by Calvo *et al.* was re-adjusted so that the linear symmetric equilibrium geometry of He_3^+ was reproduced and the model by Knowles *et al.* is based on accurate *ab initio* calculations performed for a broad range of configurations of He_3^+ performed for both the electronic ground state and two lowest excited states.

The vertical excitation energies for transitions from the electronic ground state of He_3^+ to the two lowest excited states and the corresponding transition dipole moments are summarized for classical equilibrium geometries of He_3^+ in Table II. The very good performance of the model by Knowles *et al*, already seen for the electronic ground state in Table I, is further confirmed for both excited states. The excitation energies as well as the corresponding transition dipole moments are for this model very close to accurate *ab initio* predictions. The model by Calvo *et al*, on the other hand, strongly underestimates the first excitation energy (by about 1.27 eV), which seems to indicate that (at least) the first excited state PES of He_3^+ is not well described within this model. The transition dipole moments are, on the contrary, reproduced very well. It is important to remember here that within both the model

TABLE II. Vertical excitation energies and transition dipole moments calculated for the two lowest excited states of He_3^+ in the equilibrium geometry using semiempirical models and compared with *ab initio* values (vertical energies are taken from Ref. 52 and transition dipole moments have been calculated within the present work). In parentheses, values corresponding to the equilibrium geometry obtained from the *ab initio* calculation ($r_{12} = r_{23} = 1.238$ Å) are shown for comparison. Energies are given in eV and transition dipole moments in atomic units.

Model	$\Delta E_{0\to1}$	$\Delta E_{0\to2}$	$\mu_{0\to1}$	$\mu_{0\to2}$
Knowles *et al.*	5.614 (5.651)	9.853 (9.917)	1.617 (1.613)	0.000 (0.000)
Calvo *et al.*	4.350 (4.372)	9.716 (9.772)	1.677 (1.674)	0.000 (0.000)
DIM	5.242 (4.730)	10.000 (9.819)	0.465 (1.614)	0.980 (0.000)
Ab initio	5.625	9.877	1.595	0.000

TABLE III. Charge delocalization of the electronic ground state and the two lowest excited states of equilibrium He_3^+. Charges are given in percent of e.

Model	Ground state	1st excited state	2nd excited state
Knowles *et al.*	24–52–24	50–0–50	26–48–26
Calvo *et al.*	26–48–26	50–0–50	24–52–24
DIM	49–50–1	2–0–98	50–49–1

by Knowles *et al.* and the model by Calvo *et al*, the symmetries of the wavefunctions corresponding to the electronic ground state, the first excited state, and the second excited state are, at the equilibrium linear symmetric geometry, respectively, $^2\Sigma_g^+$, $^2\Sigma_u^+$, and $^2\Sigma_g^+$. As a consequence, the transition dipole moment for the $X^2\Sigma_g^+ \rightarrow^2 \Sigma_u^+$ transition is nonzero and rather strong absorption is expected for this transition at about $E_{\text{phot}} \approx 5.62$ eV ($\lambda \approx 220$ nm, mid-UV range). Noteworthy, this conclusion conforms well with the experimental findings that a strong photoabsorption band exists for He_3^+ at $E_{\text{phot}} \approx 5.34 - 0.1/ + 0.2$ eV,[6] Only faint photoabsorption will accompany, on the other hand, the weakly forbidden transition $X^2\Sigma_g^+ \rightarrow 2^2\Sigma_g^+$ at $E_{\text{phot}} \approx 9.88$ eV ($\lambda \approx 125$ nm, far-UV range). This transition will become allowed only in vibrationally excited He_3^+, mainly because of asymmetric deformations leading to dimer-like structures, $He_2^+ \cdots He$. Interestingly, the pure DIM model gives both excitation energies rather close to the *ab initio* predictions. Merely the transition dipole moments are not well reproduced by the DIM model at the DIM equilibrium geometry. This is not surprising since the DIM geometry considerably differs from what is obtained from *ab initio* calculations. Nevertheless, if the *ab initio* equilibrium geometry is used in DIM calculations, the transition dipole moments are well reproduced for both transitions.

In Table III, the charge delocalization is overviewed for completeness for the electronic ground state and the two lowest excited states of He_3^+. For the two more realistic models, Knowles *et al.* and Calvo *et al*, similar charge delocalizations are obtained for the electronic ground state as well as for both excited states, closely following the symmetries of the corresponding electronic wavefunctions. For the DIM model, for which a linear asymmetric equilibrium geometry is predicted for the ground-state He_3^+, the charge distribution over the trimer is different. Within this model, the positive charge condenses on a dimer core in the electronic ground state with the corresponding dimer wavefunction being of approximately the $^2\Sigma_u^+$ symmetry. In the 1st excited state, the charge moves almost completely to the originally neutral atom forming a $He_2 \cdots He^+(^2S)$ structure, and, finally, returns back to the dimer core again in the 2nd excited state, the corresponding dimer wavefunction now receiving the $^2\Sigma_g^+$ symmetry. As a consequence, strong absorption is expected for the DIM model in the far-UV region corresponding to the $X^2\Sigma_u^+ \rightarrow 1^2\Sigma_g^+$ transition in the dimer core.

In the remaining parts of this section, the photoabsorption spectra calculated within the two realistic models (Knowles *et al.* and Calvo *et al.*) will be presented. First, a detailed analysis of the He_3^+ photoabsorption in the mid-UV region, for which comprehensive experimental results are available, is given, and then, the He_3^+ photoabsorption in the far-UV region is briefly analyzed. Finally, the effect of trimer vibrational and rotational excitations is briefly analyzed.

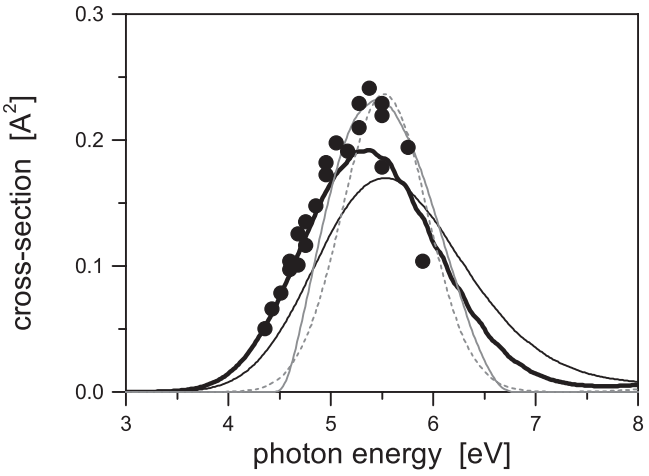

FIG. 2. Photoabsorption spectrum of He_3^+ in the mid-UV region calculated for the model by Knowles *et al.* and various nuclear configurations sampling methods: black thick line—exact ground-state rotational-vibrational wavefunction obtained from the hyperspherical approach (HYP), black thin line—harmonic ground-state rotational-vibrational wavefunction (HA), grey solid line—classical microcanonical Monte Carlo (μcMCJ0) sampling for $E_{\text{int}} = 0.80 \times$ ZPE, grey dashed line—classical canonical Monte Carlo (cMCJ0) sampling for $T = 280$ K, and bullets—experiment.[6]

A. Middle UV region

Comparisons of theoretical predictions of the He_3^+ photoabsorption cross-sections with experimental points are given in Fig. 2 for the model by Knowles *et al.* and in Fig. 3 for the model by Calvo *et al.* The DIM model is not

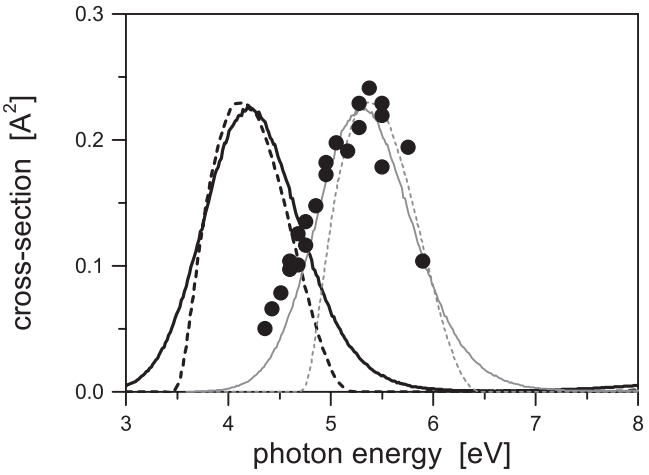

FIG. 3. Photoabsorption spectrum of He_3^+ in the mid-UV region calculated for the model by Calvo *et al.* and various nuclear configurations sampling methods: black solid line—harmonic ground-state rotational-vibrational wavefunction (HA), black dashed line—classical microcanonical Monte Carlo (μcMCJ0) sampling for $E_{\text{int}} =$ ZPE, grey solid line—as black solid line, but shifted by +1.1 eV along the photon energy axis, grey dashed line—as black dashed line, but shifted by +1.26 eV along the photon energy axis, and bullets—experiment.[6]

TABLE IV. Positions, halfwidths, and heights of theoretical profiles of the photoabsorption band of He_3^+ in the mid-UV region as obtained for the model by Knowles *et al.* and compared with experiment. Photon energies (position and halfwidth) are given in eV, cross-sections (height) are given in Å^2. Uncertainties for position, halfwidth, and height of the experimental profile are, respectively, $-0.1/+0.2$ eV, $-0.05/+0.1$ eV, and $-0.1/+0.2$ Å^2.[6]

Model	Position	Halfwidth	Height
HYP	5.36	0.66	0.19
HA	5.55	0.75	0.17
μcMCJ0	5.47	0.55	0.23
cMCJ0	5.53	0.42	0.23
Experiment	5.34	0.57	0.22

included since it leads to essentially zero photoabsorption cross-sections in this range.

In calculations performed for the Knowles *et al.* model, several approaches for sampling the nuclear configurations used to model nuclear delocalization effects have been employed: (a) sampling from the exact nuclear wavefunction (HYP, Subsection II C 1) which we consider a benchmark for the other calculations, (b) sampling from the harmonic nuclear wavefunction (HA, Subsection II C 2), and (c) two classical sampling algorithms based on the Monte Carlo methodology (cMCJ0 and μcMCJ0, Subsection II C 3). In the classical sampling calculations, effective temperature and/or He_3^+ internal vibration energy were used that best reproduce the height of the experimental peak, $T = 280$ K for the canonical sampling (cMCJ0)[53] and $E_{int} = 0.80 \times$ ZPE (ZPE abbreviates the Zero Point Energy) for the microcanonical sampling (μcMCJ0). The following conclusions are clear from Fig. 2 and Table IV. First, the position of the experimental peak ($E_{phot} \approx 5.34$ eV) is well reproduced by all the sampling approaches considered. A slight shift of the HA and cMCJ0 curves towards a bit larger photon energies may result from the fact that configurations with shorter distances, lying on the repulsive part of the He_3^+ PES, are slightly overestimated by these two methods. Second, both quantum samplings (HYP and HA) reproduce well the height of the experimental mid-UV peak, the experimental peak being only by about 15% higher than the height resulting from the benchmark HYP approach. Note that the excellent correspondence between the experimental peak height and the height of the cMCJ0 and μcMCJ0 profiles is an artifact of the calculation strategy since the height of the theoretical profiles has been adjusted by changing the He_3^+ temperature and/or internal vibrational energy to fit the height of the experimental peak. Third, the width of the mid-UV absorption peak is slightly overestimated by the quantum sampling methods (HYP and HA) and underestimated by the classical sampling methods (particularly by cMCJ0). But, in general the correspondence between theoretical predictions and the width of the mid-UV peak obtained from a fit of experimental points is fairly good. As already partly discussed in remark,[53] the sharper shape of theoretical absorption profiles obtained for classical samplings is probably the consequence of insufficient sampling of the nuclear configurations beyond the classical turning points in classical sampling schemes. For cMCJ0, for example, the temperature best reproducing the peak height is too low to sample properly the symmetric stretching of He_3^+, the mode which is expected to be particularly important in the mid-UV region photoabsorption of He_3^+. For μcMCJ0, a problem surely arises from the sampling not being able to cross the borders of the classically accessible region at a given internal energy. Despite all these reservations, one can safely conclude that the theoretical absorption profiles presented in Fig. 3 for the model by Knowles *et al.* reproduce the experimental points very well. Even the data obtained via classical sampling methods lead to a satisfactory agreement with the experiment.

Another conclusion which is obvious from Fig. 3 is that the population of He_3^+ was probably cold in the experiments of Ref. 6, their temperature having been close to zero. The following reasons lead us to this conclusion: (a) the photoabsorption profiles obtained for quantum samplings at $T = 0$ K (HYP and HA) reproduce the experimental points very well, (b) the profiles obtained for classical μcMCJ0 sampling algorithm reproduce best the experiment for the classical internal energy of He_3^+ below the quantum zero-point vibration energy, and (c) for the classical cMCJ0 approach, the simulation temperature best reproducing experimental absorption cross-sections is close to or below the effective classical temperatures for which the cMCJ0 algorithm should reproduce quantum nuclear delocalization at $T = 0$ K (cf. Ref. 53). In addition, if the temperature and/or internal vibration energy are increased in the classical simulations, the height of the photoabsorption profile decreases considerably and the theoretical prediction moves away from the experiment (see Subsection III C).

Data we have obtained in the mid-UV region for the Calvo *et al.* model are compared with experiment in Fig. 3. Only two sampling algorithms have been used for this model, namely, HA and μcMCJ0, and two sets of theoretical curves are presented in Fig. 3, black curves displaying direct computational data and grey curves representing the computational data shifted along the photon energy axis. As expected from the data given in Table II, the position of the mid-UV photoabsorption of He_3^+ is not well reproduced within the model by Calvo *et al.* Namely, while the width and the height of the two theoretical peaks are in good correspondence with the experiment, in particular for the HA sampling method (see Table V), the theoretical prediction of the band position is not. But, if the theoretical profiles are shifted properly along the energy axis (grey curves in Fig. 3), almost perfect agreement with the experimental photoabsorption spectrum is achieved. The needed shifts are $\Delta E_{phot} \approx 1.10$ eV for HA and $\Delta E_{phot} \approx 1.26$ eV for μcMCJ0. As already discussed above, the modifications of the He_3^+ ground-state PES employed in the model by Calvo *et al.* to reproduce the He_3^+

TABLE V. As in Table IV, but calculated for the model by Calvo *et al.*

Model	Position	Halfwidth	Height
HA	4.21	0.56	0.22
μcMCJ0	4.15	0.41	0.23
Experiment	5.34	0.57	0.22

equilibrium geometry may not be appropriate for the 1st excited state. Nevertheless, it seems that the 1st excited PES has a correct shape in this model and is only shifted by some more or less constant value (about 1.1–1.3 eV) to lower the interaction energies.

The data we obtained in the mid-UV region using the DIM model (not graphically represented here) clearly document the failure of this model for He_3^+. Although a weak absorption band has been detected in μcMCJ0 calculations on the trimer excited at E_{int} = ZPE at $E_{phot} \approx 4.8$ eV (cf. Table II), the height of the band is about 200 times lower than the value resulting from the experiment; the corresponding photoabsorption cross-sections are, thus, essentially zero within the pure DIM model. Since the DIM model does not describe the ground-state PES of He_3^+ well and prefers asymmetric dimer-like structures, the photoabsorption profile produced for He_3^+ by this approach is close to the dimer photoabsorption profile which is also close to zero in the mid-UV range. Only for non-physically frozen trimer (E_{int} = 1 meV $\approx$0.01 × ZPE), the height of the theoretical peak calculated using the pure DIM model ($\approx$0.23 Å^2) and its position ($E_{phot} \approx 5.24$ eV) become comparable to the height and position of the experimental peak. However, an extremely narrow theoretical profile is obtained in this extreme case.

B. Far UV region

It is clear from Table II that additional absorption peak can be expected for He_3^+ in the far-UV region at around $E_{phot} \approx 10$ eV. Since there are no experimental data on the He_3^+ photoabsorption in this region, only theoretical predictions resulting from various approaches are compared here. This is done in Fig. 4 and Table VI for the models by Knowles *et al.* and Calvo *et al.* and for two quantum sampling algorithms (HA and HYP). Since mainly asymmetric deformations of He_3^+ leading to dimer-like structures, $He_2^+ \cdots He$, are expected to be responsible for the absorption of He_3^+ in the far-UV region, photoabsorption spectrum of He_2^+ (calculated using the diatomic potentials for He_2^+ taken from the two models involved) is also considered for comparison.

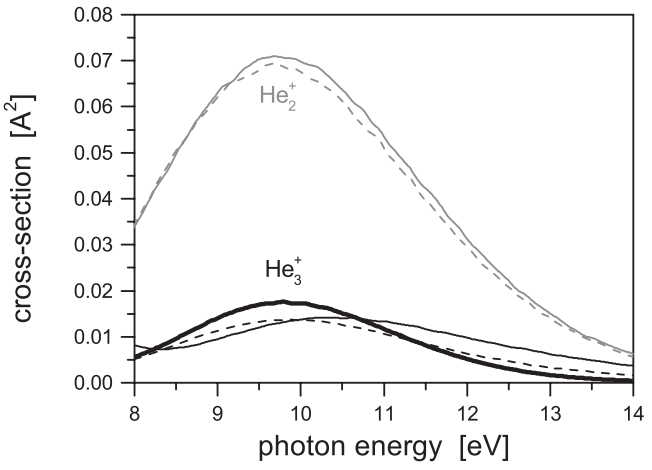

FIG. 4. Photoabsorption spectrum of He_3^+ calculated for various models (black lines) in the far-UV region and compared with the photoabsorption spectrum of He_2^+ (grey lines): thick solid line—exact ground-state rotational-vibrational wavefunction obtained from the hyperspherical approach (HYP) and the model by Knowles *et al.* (only He_3^+), thin solid line—harmonic ground-state rotational-vibrational wavefunction (HA) and the model by Knowles *et al.*, dashed line—harmonic ground-state rotational-vibrational wavefunction (HA) and the model by Calvo *et al.*

TABLE VI. Positions, halfwidths, and heights of theoretical profiles of the photoabsorption band of He_3^+ in the far-UV region. Photon energies (position and halfwidth) are given in eV and cross-sections (height) in Å^2.

Model	Position	Halfwidth	Height
Knowles *et al.* and HYP	9.85	1.28	0.017
Knowles *et al.* and HA	10.46	1.69	0.014
Calvo *et al.* and HA	9.93	1.50	0.014
He_2^+(Calvo *et al.*)	9.85	1.60	0.071
He_2^+(Knowles *et al.*)	9.79	1.61	0.069

After inspecting Fig. 4 and Table VI, one can conclude that a considerably broader and more than ten times weaker band is predicted for the far-UV region comparing to the photoabsorption profiles reported for He_3^+ in the mid-UV range. All the three theoretical models considered in Fig. 4 provide qualitatively as well as quantitatively comparable absorption profiles with the position of the absorption band varying between $E_{phot} \approx 9.8$ eV and $E_{phot} \approx 10.5$ eV, height ranging between 0.014 Å^2 and 0.018 Å^2, and with halfwidth being between 1.3 eV to 1.7 eV. The far-UV absorption band of He_3^+ is qualitatively similar to the corresponding band of He_2^+, the latter being about 4–5 times stronger. The similarity between the dimer and trimer photoabsorption spectrum can be rather easily understood since mainly asymmetric deformations of the equilibrium geometry of He_3^+ are responsible for its far-UV photoabsorption, i.e., mostly $He_2^+ \cdots He$ configurations contribute. The differences between the profiles obtained for He_3^+ and for He_2^+ are, on the other hand, due to solvation effects by the third atom in He_3^+, mainly due to different charge redistributions in respective excited electronic states of the two species.

C. Effect of vibrational and rotational excitations

How the photoabsorption of He_3^+ is influenced by the vibrational excitations of the trimer has been investigated at the classical level for the model by Knowles *et al.* by employing μcMCJ0 sampling method with several choices of trimer vibrational energy. The results are summarized in Fig. 5 where, together with the photoabsorption profile best reproducing the experimental data (E_{int} = 0.80 × ZPE, grey curve), photoabsorption profiles are displayed also for higher vibrational energies (black curves) ranging between E_{int} = ZPE and E_{int} = ZPE + 60 meV. It is worth emphasizing that ZPE = 113 meV for He_3^+ within the model by Knowles *et al.* and that the dissociation energy for He_2^+ + He is E_{diss} = 189 meV in this case, i.e., only 76 meV above the ZPE level. The highest vibrational energy considered in Fig. 5 is thus close to the dissociation limit and the vibrational energies considered here cover almost completely the whole range of possible vibrational excitations of He_3^+.

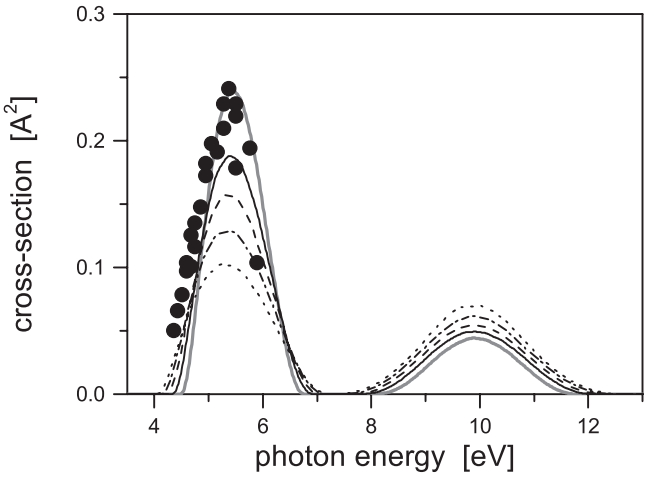

FIG. 5. Photoabsorption spectrum of He_3^+ calculated for various vibrational excitations using the model by Knowles *et al.* and the classical microcanonical Monte Carlo (μcMCJ0) sampling method: solid line—E_{int} = ZPE, dashed line—E_{int} = ZPE + 20 meV, dashed-dotted line—E_{int} = ZPE + 40 meV, and dotted line—E_{int} = ZPE + 60 meV (about 15 meV below the He_2^+ + He dissociation limit). For comparison, the μcMCJ0 photoabsorption profile of Fig. 2 best reproducing experimental data (thick grey line) and the experimental points[6] (bullets) are also included.

In the mid-UV region, several systematic trends are observed in the evolution of the photoabsorption spectrum with increasing vibrational energy of He_3^+. First of all, the height of the mid-UV band decreases considerably (from 0.23 Å^2 at E_{int} = 0.80 × ZPE to 0.10 Å^2 at E_{int} = ZPE + 60 meV) if the vibrational excitation increases. This is quite understandable since mainly symmetric configurations contribute in this range of photon energies and the symmetry of He_3^+ is heavily disturbed towards asymmetric geometries in vibrationally hot trimers. Second, the asymmetry of the band becomes more apparent for higher excitations with, third, the maximum shifting gradually to lower photon energies (from 5.47 eV at E_{int} = 0.80 × ZPE down to 5.35 eV at E_{int} = ZPE + 60 meV). Both latter effects are attributed to anharmonic features of the He_3^+ PES.

The trends are completely different in the far-UV region. The height of the far-UV band increases with increased He_3^+ vibrational excitation, the symmetry of the band is more or less preserved, and only negligible shift of the far-UV band is observed along the photon energy axis (from about 9.9 eV at E_{int} = 0.80 × ZPE to approximately 9.87 eV at the highest E_{int} considered). The most pronounced trend is thus the increase of the height of the far-UV band with increased vibrational excitation of He_3^+ (from 0.044 Å^2 at E_{int} = 0.80 × ZPE to 0.070 Å^2 at E_{int} = ZPE + 60 meV[54]). This evolution has basically the same origin as the well apparent decrease of the height of the mid-UV band. Because asymmetric, dimer-like configurations of He_3^+ are dominantly responsible for the photoabsorption of the cluster in the far-UV and because asymmetric distortions of He_3^+ become more frequent at higher vibrational excitations, it is not surprising that the photoabsorption is enhanced in this region of photon energies for vibrationally excited He_3^+.

Another interesting observation is that the best correspondence between experimental cross-sections recorded in the mid-UV region and the theoretical predictions obtained from classical, μcMCJ0 calculations is obtained for the vibrational energy of He_3^+ considerably below the ZPE (E_{int} = 0.80 × ZPE), while for E_{int} = ZPE, the classical photoabsorption cross-sections correspond rather well to the quantum simulations performed for the vibrationally ground-state He_3^+. For example, the height of the mid-UV band is 0.19 Å^2 for μcMCJ0 and E_{int} = ZPE, 0.19 Å^2 for HYP calculations, and 0.17 Å^2 for HA calculations.

The effect of rotational excitations of He_3^+ on its photoabsorption spectrum has also been preliminarily investigated by comparing the results of μcMCJ0 calculations performed for three lowest vibrational energies considered in this work (E_{int} = 0.80 × ZPE, E_{int} = ZPE, and E_{int} = ZPE + 20 meV) with the results obtained from classical microcanonical Monte Carlo simulations with the rotational degrees of freedom of He_3^+ included (μcMCJ≠0),[50,51]

$$\rho(\mathbf{R})_{\mu c,J\neq 0} \sim [E_{int} - E_0(\mathbf{R})]^{\frac{f}{2}-1}\Theta[E_{int} - E_0(\mathbf{R})], \qquad (11)$$

where f is the number of internal, both vibrational and rotational degrees of freedom (f = 6 for He_3^+), and with internal energies multiplied by a factor 5/4. This factor has been derived from the assumption that the internal energy is distributed among 2 rotations and 4 vibrations of rotating He_3^+ following the classical equipartition theorem and that the amount of internal energy per one rotation degree of freedom is equal, within the classical treatment, to 1/2 of the average amount of internal energy stored in one vibrational mode. The result of such comparison is shown in Fig. 6 from which it is clear that the trends observed for vibrationally excited He_3^+ are further magnified if trimer rotations are involved, in particular in the far-UV range of photon energies. In the mid-UV range, the effect of rotational excitations in He_3^+ on the

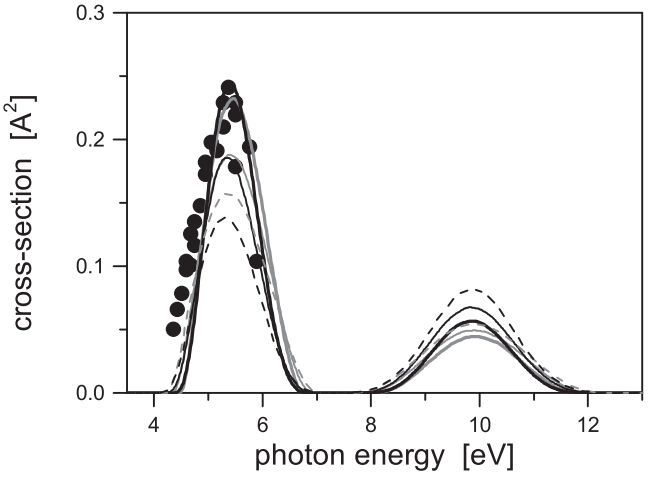

FIG. 6. Photoabsorption spectrum of He_3^+ calculated for three selected rotational-vibrational excitations using the model by Knowles *et al.* and the classical microcanonical Monte Carlo sampling method with the inclusion of cluster rotations (Eq. (11), black lines) compared to data obtained for non-rotating clusters (Eq. (10), grey lines): thick black line—rotating clusters with E_{int} = 5/4 × (0.80 ZPE), thick grey line—non-rotating clusters with E_{int} = 0.80 ZPE, thin black line—rotating clusters with E_{int} = 5/4 × ZPE, thin grey line—non-rotating clusters with E_{int} = ZPE, dashed black line—rotating clusters with E_{int} = 5/4 × (ZPE + 20 meV), dashed grey line—non-rotating clusters with E_{int} = ZPE + 20 meV, and bullets—experimental points.[6]

height of the photoabsorption peak becomes significant only for higher internal energies. But, narrower absorption profiles shifted slightly toward lower photon energies are obtained in this range if He_3^+ rotations are included. Taking into account the fact that the $J = 0$ weight (Eq. (10)) prefers close-to-linear configurations due to the presence of the inertia matrix determinant in the denominator of the r.h.s. of Eq. (10), the shift can probably be attributed to the enhanced abundance of nonlinear structures in $J \neq 0$ simulations. In addition, the distances between particles become larger in rotating systems due to centrifugal forces, which is further expected to cause a slight shift of excitation energies in He_3^+ toward lower values.

IV. CONCLUSIONS

Photoabsorption of the helium trimer cation, He_3^+, has been studied theoretically using various interaction models and various methods for modeling nuclear delocalization effects. The models used for the modeling of intracluster interactions are based on the DIM approach[17] and include three-body interactions either via explicit three-body corrections to the DIM Hamiltonian as described in Refs. 21 and 25 (the Knowles *et al.* model) or by using effective diatomic potentials as introduced in Ref. 23 and developed further by Calvo *et al.* in Ref. 24 (denoted here as the Calvo *et al.* model). For comparison, a pure DIM model has also been considered. The methods used for modeling the nuclear delocalization effects are based on ground-state rotational-vibrational wavefunctions obtained either from an exact solution of the nuclear Schrödinger equation via the HYP approach[37,38] or at the HA level,[13] or from classical samplings using canonical and microcanonical Monte Carlo methods.[50,51] A simple *point-charge approximation*[10] has been used for the calculation of transition probabilities (transition dipole moments)[11] since it has been proven sufficiently accurate by a direct comparison of the transition dipole moments obtained for a broad range of interatomic distances in He_2^+ within this approximation and via accurate *ab initio* calculations.

According to theoretical predictions, two photoabsorption bands exist in the He_3^+ spectrum, one in the mid-UV region (around $E_{phot} \approx 5.5$ eV) and another, much weaker, in the far-UV region (around $E_{phot} \approx 10$ eV). Theoretical results obtained for the mid-UV range may serve as a test of the theoretical approaches employed since comprehensive experimental data are available here.[6]

In general, a very good correspondence with the experimental data has been achieved for the model by Knowles *et al.* The most accurate method for the inclusion of nuclear delocalization, HYP, combined with this interaction model reproduces well the position of the mid-UV band, only slightly underestimates its height, and slightly overestimates the width of the peak. The other quantum method for modeling the nuclear delocalization, the HA approach, also reproduces the experimental points fairly well leading to a position of the mid-UV band shifted by about 0.2 eV to higher photon energies, slightly overestimating the width of the band, and underestimating a bit its height. Interestingly, both classical sampling methods, canonical and microcanonical Monte Carlo, reproduce the experimental photoabsorption profiles well if classical internal energy and/or temperature of He_3^+ are set properly in simulations. The only visible discrepancy, but still not very important, is seen on the lower energy shoulder of the mid-UV peak where the classical sampling underestimates experimental cross-sections. In summary, the model by Knowles *et al.* seems to provide a reliable electronic Hamiltonian for He_3^+ and provides realistic description of both the electronic ground state and the lowest excited states of He_3^+.

The situation is more ambiguous for the model of Calvo *et al.* In the mid-UV region, the theoretical predictions of He_3^+ photoabsorption cross-sections are shifted by about 1.1–1.3 eV to lower photon energies. A natural reason of this inconsistency may be that the effective modifications of the DIM Hamiltonian of He_3^+ embedded in the model by Calvo *et al.* have been considered only for the electronic ground state. It means, that even if the model reproduces the electronic ground state of He_3^+ well (as documented, e.g., by the correct equilibrium geometry of He_3^+ predicted by this model), it need not be as much reliable for excited states. An overall lesson that can be drawn from the comparison between the models by Calvo *et al.* and Knowles *et al.* is that the three-body corrections to the He_3^+ DIM Hamiltonian, either effective or explicit, must be considered not only for the electronic ground state but also for all the excited states that are involved. More generally, modifications of only one of the potential energy surfaces may not be sufficient. It is worth emphasizing, however, that if the theoretical photoabsorption profiles calculated for the model by Calvo *et al.* are just properly shifted to larger photon energies, they reproduce the experimental points excellently. This may indicate that the PES for the first excited state has a correct shape and is only shifted downwards along the energy axis with respect to true values.

As expected, the DIM model fails in the mid-UV range and it predicts an extremely weak photoabsorption band in this range (about 200 times weaker than the experimental one). On the other hand, the peak has a correct position. It may mean that the pure DIM model fails mainly due to the distorted shape of the electronic ground-state PES leading to an incorrect preference of asymmetric $He_2^+ \cdots He$ configurations, but provides rather good vertical excitation spacings.

Another conclusion which is clear from the comparison of the theoretical predictions with experimental data in the mid-UV range and which is worth emphasizing here is that the ionized trimers of helium involved in the experiment of Ref. 6 must have been rather cold. Such a conclusion is strongly supported by the fact that the theoretical data obtained from zero-temperature (quantum) samplings compare very well with the experimental points.

In the far-UV range, both the model by Knowles *et al.* and the model by Calvo *et al.* predict a weak and broad photoabsorption band at $E_{phot} \approx 10$ eV. The band is about 10 times weaker than the band detected in the mid-UV region and resembles qualitatively the photoabsorption profile of He_2^+. This can be well understood since asymmetric deformations of the equilibrium geometry of of He_3^+ are responsible for its far-UV photoabsorption, i.e., mostly $He_2^+ \cdots He$ configurations contribute. The difference between the He_2^+ and He_3^+ absorption

profiles (the dimer photoabsorption is about 3–4 times higher, see Fig. 4) is due to the solvation effect of the third atom in He_3^+, in particular, due to different charge re-distribution in respective excited states of He_2^+ and He_3^+.

The effect of internal (vibrational and rotational) excitations on the photoabsorption spectrum of He_3^+ has been investigated at the classical level and for the model by Knowles *et al.* It has been found that vibrational excitations considerably decrease the height of the absorption band in the mid-UV range and, on the other hand, increase the height of the band in the far-UV range. This major effect can be interpreted in terms of the increased abundance of asymmetric configurations in the population of vibrationally excited helium trimer cations. The main reason for this is that the asymmetric, dimer-like structures are responsible for the photoabsorption of He_3^+ in the far-UV region while more or less symmetric structures exhibit strong photoabsorption in the mid-UV range where the asymmetric species absorb only weakly. If rotational excitations are considered, the trend observed for vibrational excitations is further magnified. A major observation concerning the role of rovibrational excitations in He_3^+ is that the photoabsorption profiles calculated for vibrationally and rotationally excited cationic trimers of helium deviate significantly from the experimental points reported in the mid-UV range.[6] This seems to further support the conclusion we give above in this section, namely, that the experimental population of He_3^+ was rather cold.

A general conclusion of this work may be that the simulation methods based on the model of Knowles *et al.* for intracluster interactions, proper modelings of nuclear delocalization effects, and *point-charge approximation* for the evaluation of transition probabilities perform well in calculations of the photoabsorption spectrum of He_3^+ and represent, thus, useful tools for similar studies on larger ionic helium clusters as well as for studies on their photodissociation. Such work is presently under preparation and will be a subject of prospective studies. The Calvo *et al.* model must be, on the other hand, used with care whenever excited states of He_N^+ are involved since the excited states may not be described correctly within this model.

ACKNOWLEDGMENTS

This work has been financially supported by the Operational Programme *Research and Development for Innovations* funded by Structural Funds of the European Union and the state budget of the Czech Republic (Grants Nos. CZ.1.05/1.1.00/02.0070 and CZ.1.05/2.1.00/03.0058) and by the Ministry of Education, Youth and Sports of the Czech Republic (Grants Nos. LM2011033, 7E12028, and MSM6198910027). F.K. and B.L. further acknowledge financial support from the Barrande programme of French-Czech cooperation (Grant No. 7AMB12FR026), and F.K. expresses his thanks to the Operational Program Education for Competitiveness - European Social Fund (Grants Nos. CZ.1.07/2.3.00/20.0017 and CZ.1.07/2.3.00/20.0058) for partial financial support. The calculations were performed on the computers of the Supercomputing Center of the Technical University of Ostrava.

[1]The number of experimental and theoretical studies reported on this subject in the literature is fairly large and a very incomplete selection of them can be cited here. Since the main focus of the present paper is on the photoabsorption of the ionic helium trimer, only studies dealing with the photoabsorption of ionic rare-gas trimers are considered.
[2]N. E. Levinger, D. Ray, M. L. Alexander, and W. C. Lineberger, J. Chem. Phys. **89**, 5654 (1988).
[3]M. Deluca and M. A. Johnson, Chem. Phys. Lett. **162**, 445 (1989).
[4]Z. Y. Chen, C. D. Cogley, J. H. Hendricks, B. D. May, and A. W. Castleman, J. Chem. Phys. **93**, 3215 (1990).
[5]H. Haberland, B. von Issendorf, T. Kolar, H. Kommeier, C. Ludewigt, and A. Risch, Phys. Rev. Lett. **67**, 3290 (1991).
[6]H. Haberland and B. von Issendorff, J. Chem. Phys. **102**, 8773 (1995).
[7]H. H. Michels, R. H. Hobs, and L. A. Wright, Appl. Phys. Lett. **35**, 153 (1979).
[8]W. R. Wadt, Appl. Phys. Lett. **38**, 1030 (1981).
[9]F. X. Gadea and M. Amarouche, Chem. Phys. **140**, 385 (1990).
[10]T. Ikegami, T. Kondow, and S. Iwata, J. Chem. Phys. **98**, 3038 (1993).
[11]F. X. Gadea and M. Amarouche, J. Phys. II (France) **5**, 1767 (1995).
[12]A. Bastida and F. X. Gadea, Chem. Phys. **209**, 291 (1996).
[13]N. L. Doltsinis and P. J. Knowles, Chem. Phys. Lett. **301**, 241 (1999).
[14]N. Doltsinis, Mol. Phys. **97**, 847 (1999).
[15]R. Kalus and D. Hrivňák, Chem. Phys. **278**, 21 (2002).
[16]R. Kalus, I. Paidarová, D. Hrivňák, and F. X. Gadea, Chem. Phys. **298**, 155 (2004).
[17]F. O. Ellison, J. Am. Chem. Soc. **85**, 3540 (1963).
[18]P. Milko, R. Kalus, I. Paidarová, J. Hrušák, and F. X. Gadea, Theor. Chem. Acc. **124**, 169 (2009).
[19]M. Amarouche, G. Durand, and J. P. Malrieu, J. Chem. Phys. **88**, 1010 (1988).
[20]J. S. Cohen and B. I. Schneider, J. Chem. Phys. **61**, 3230 (1974).
[21]P. J. Knowles, J. M. Murrell, and E. J. Hodge, Mol. Phys. **85**, 243 (1995).
[22]F. X. Gadea and I. Paidarová, Chem. Phys. **209**, 281 (1996).
[23]M. Ovchinnikov, B. L. Grigorenko, K. C. Janda, and V. A. Apkarian, J. Chem. Phys. **108**, 9351 (1998).
[24]F. Calvo, F. Y. Naumkin, and D. J. Wales, J. Chem. Phys. **135**, 124308 (2011).
[25]P. J. Knowles and J. M. Murrell, Mol. Phys. **87**, 827 (1996).
[26]T. Ikegami and S. Iwata, J. Chem. Phys. **105**, 10734 (1996).
[27]W. J. Stevens, M. Gardner, A. Karo, and P. Julienne, J. Chem. Phys. **67**, 2860 (1977).
[28]E. J. Heller, J. Chem. Phys. **68**, 2066 (1978).
[29]R. Schinke, *Photodissociation Dynamics: Spectroscopy and Fragmentation of Small Polyatomic Molecules* (Cambridge University Press, Cambridge, 1993).
[30]P. J. Kuntz and J. Valldorf, Z. Phys. D **8**, 195 (1988).
[31]N. L. Doltsinis and P. J. Knowles, Mol. Phys. **94**, 981 (1998).
[32]J. Xie, B. Poirier, and G. I. Gellene, J. Chem. Phys. **122**, 184310 (2005).
[33]R. A. Aziz, A. R. Janzen, and M. R. Moldover, Phys. Rev. Lett. **74**, 1586 (1995).
[34]F. Y. Naumkin, Chem. Phys. **252**, 301 (2000).
[35]H.-J. Werner, P. J. Knowles, R. Lindh, F. R. Manby, M. Schütz *et al.*, MOLPRO, version 2012.1, a package of *ab initio* programs, 2012, see http://www.molpro.net.
[36]This assumption will be partly verified in Sec. III where photoabsorption spectra calculated for He_3^+ in the mid-UV region will be compared with experimental points and good agreement will be achieved.
[37]A. Kuppermann, J. Phys. Chem. **100**, 2621 (1996).
[38]D. Wang and A. Kuppermann, J. Phys. Chem. A **107**, 7290 (2003).
[39]F. Karlický, B. Lepetit, R. Kalus, I. Paidarová, and F. X. Gadea, J. Chem. Phys. **128**, 124303 (2008).
[40]F. Karlický, B. Lepetit, R. Kalus, and F. X. Gadea, J. Chem. Phys. **134**, 084305 (2011).
[41]F. Karlický, B. Lepetit, R. Kalus, and F. X. Gadea, J. Chem. Phys. **126**, 174305 (2007).
[42]L. Velilla, B. Lepetit, A. Aguado, J. A. Beswick, and M. Paniagua, J. Chem. Phys. **129**, 084307 (2008).
[43]As we are dealing with the ground vibrational state, geometric phase effects which become significant for excited states can be neglected.[39] Test calculations of photoabsorption profiles of He_3^+ we performed with and without the inclusion of the geometric phase (not reported here) fully confirm this assumption.

[44]In fact, the Jacobian for the hyperspherical to Cartesian coordinates transition, $J_{H\rightarrow C} \equiv \det[\partial \mathbf{R}_C/\partial \mathbf{R}_H]$, reads as follows, $J_{H\rightarrow C} = 1/4\rho^5 \sin(b)\sin(4\theta)$. In Eq. (7), we omit irrelevant constant factor 1/4, as well as factor $\sin(b)$ which need not be considered in a non-rotating system.

[45]J. Goodisman, *Contemporary Quantum Chemistry. An Introduction* (Plenum Press, New York, 1977), Chap. 5.1, pages 83–86.

[46]The four normal vibrational modes considered in Eq. (8) are a symmetric stretching mode, an asymmetric stretching mode, and a doubly degenerate bending mode. The frequencies and directions of these four vibrational modes are obtained by diagonalizing the 9×9 Hessian matrix calculated at the equilibrium, linear symmetric configuration of He_3^+. Four non-zero eigenvalues of the matrix and corresponding eigenvectors lead to the vibrational modes, five zero eigenvalues correspond to the translation and rotation of the cluster as a whole.

[47]A problem may arise if more than one vibrational modes with considerably different frequencies are involved. In that case, a classical constant-temperature simulation will reproduce quantum nuclear delocalization only loosely.

[48]D. P. Landau and K. Binder, *A Guide to Monte Carlo Simulations in Statistical Physics* (Cambridge University Press, Cambridge, 2000).

[49]N. Metropolis, A. W. Rosenbluth, M. N. Rosenbluth, A. H. Teller, and E. Teller, J. Chem. Phys. **21**, 1087 (1953).

[50]G. Nyman, S. Nordholm, and H. W. Schranz, J. Chem. Phys. **93**, 6767 (1990).

[51]F. Calvo, J. Galindez, and F. X. Gadea, J. Phys. Chem. A **106**, 4145 (2002).

[52]I. Paidarová, R. Polák, B. Paulíková, F. Karlický, K. Oleksy, D. Hrivňák, F. X. Gadea, and R. Kalus, Chem. Phys. **342**, 64 (2007).

[53]The effective temperatures (see Subsection II C 3) corresponding to the four normal vibrational modes of He_3^+ (symmetric stretch, asymmetric stretch, and doubly degenerate bending) are, respectively, $T_{\text{eff}}^{\text{ss}} \approx 658$ K, $T_{\text{eff}}^{\text{as}} \approx 251$ K, and $T_{\text{eff}}^{\text{bend}} \approx 203$ K. The effective temperature used in the cMCJ0 calculations to best reproduce the height of the experimental mid-UV peak compares well with $T_{\text{eff}}^{\text{as}}$ and $T_{\text{eff}}^{\text{bend}}$, but is significantly lower than $T_{\text{eff}}^{\text{ss}}$. This may be the main reason for that the cMCJ0 profile is a bit narrower than the profile recorded experimentally.

[54]Note that the height of the far-UV band predicted by classical calculations (μcMCJ0) is about three times larger than the height resulting from quantum calculations (HYP or HA). This may indicate that the abundance of asymmetric, dimer-like configurations, which are the main contributors to the far-UV absorption of He_3^+, is overestimated in the classical approach. It is further worth emphasizing that the height of the far-UV band of He_3^+ is comparable for the highest vibrational excitation considered with the height of the far-UV band of He_2^+ (*cf.* Table VI). Clearly, the dimer-like form of He_3^+ configurations is much more pronounced in highly excited trimers.